

Single exciton spectroscopy of single-Mn doped InAs quantum dots

J. van Bree,^{1,2} P.M. Koenraad,² and J. Fernández-Rossier¹

¹*Departamento de Física Aplicada, Universidad de Alicante, San Vicente del Raspeig, 03690 Spain*

²*Department of Applied Physics, Eindhoven University of Technology,
P.O. Box 513, NL-5600MB Eindhoven, The Netherlands*

(Dated: February 2, 2022)

The optical spectroscopy of a single InAs quantum dot doped with a single Mn atom is studied using a model Hamiltonian that includes the exchange interactions between the spins of the quantum dot electron-hole pair, the Mn atom and the acceptor hole. Our model permits to link the photoluminescence spectra to the Mn spin states after photon emission. We focus on the relation between the charge state of the Mn, A^0 or A^- , and the different spectra which result through either band-to-band or band-to-acceptor transitions. We consider both neutral and negatively charged dots. Our model is able to account for recent experimental results on single Mn doped InAs PL spectra and can be used to account for future experiments in GaAs quantum dots. Similarities and differences with the case of single Mn doped CdTe quantum dots are discussed.

PACS numbers:

I. INTRODUCTION

Probing a single magnetic atom in a solid state environment is now possible by scanning tunneling microscopy (STM), both in metallic¹ and semiconducting surfaces^{2,3,4,5}, and by single exciton spectroscopy in semiconductor quantum dots^{6,7,8}, among other techniques. These experiments permit to address a single quantum object, the spin of the magnetic atom, and to study its exchange interactions with surrounding carriers. Quantum dots doped with a single magnetic atom are a model system for nanospintronics^{9,10,11}. These systems can also shed light on the issue of whether or not it is possible to dope semiconductor nanocrystals¹².

The focus of this work is the single exciton spectroscopy of a single Mn atom in a InAs quantum dot (QD), motivated by recent experimental results on InAs QD⁸ and keeping in mind the relation to previous experiments on single Mn doped CdTe⁶. The photoluminescence (PL) spectra of a CdTe QD doped with only one Mn atom display six narrow peaks, each of which correspond^{6,13} to one of the six quantum states of the $S = 5/2$ multiplet formed by the 5 Mn d electrons¹⁴ in Mn^{2+} . Hence, the spin state of the single Mn atom after its interaction with an exciton in a CdTe QD can be read from the energy and polarization of the emitted photon^{6,13}. Another interesting result in CdTe dots doped with Mn, is the fact that the PL spectrum changes radically when a single carrier is electrically injected into the dot⁷. This has been explained in terms of the different effective spin Hamiltonian for the Mn as a single additional carrier is added into the dot^{7,11,15}.

Since Mn is an acceptor in InAs quantum dot, the single Mn exciton PL is expected to be different from CdTe, where Mn acts as a isoelectronic impurity. Even before photoexcitation, charge neutrality implies that the Mn acceptor in InAs binds a hole. In this neutral acceptor complex, A^0 , the spin of the Mn is antiferromagnetically coupled to the spin of the acceptor hole, so that A^0 be-

haves as effective spin $F = 1$ object. When a neutral exciton X^0 is created in a InAs dot doped with 1 Mn, there are 4 spins interacting: the QD electron, the QD hole, the Mn and the acceptor hole. Indeed, recent experimental observations report a band-to-band transition ($X^0 A^0 \rightarrow A^0$) PL spectrum with 5 peaks with different intensities at zero applied field, instead of the 6 almost identical peaks in CdTe. The presence of the acceptor hole also opens a new optical recombination channel, the band-to-acceptor transition ($X^0 A^0 \rightarrow h^+ A^-$) such that the conduction band electron ionizes the Mn acceptor without filling the quantum dot hole.

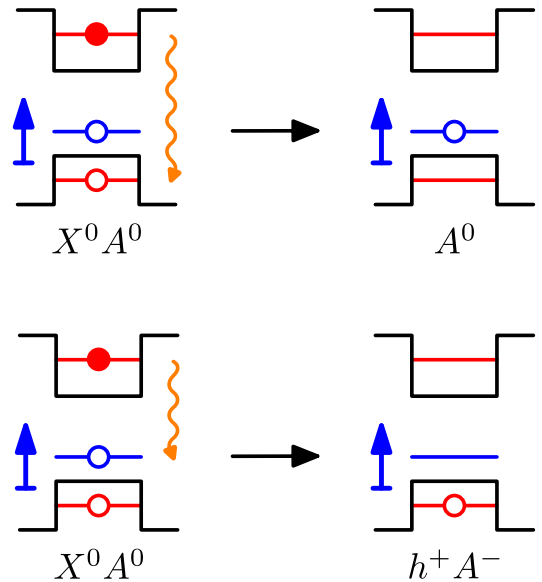


FIG. 1: Schematic energy levels of the InAs dot doped with 1 Mn. Upper row: band-to-band transition. Lower row: band-to-acceptor transition. (Color online)

The goal of this paper is to provide a theoretical framework to understand the relation between PL spectra of a single InAs quantum dot doped with one Mn and the

interactions, charge and spin state of the relevant degrees of freedom. The rest of this paper is organized as follows. In section II we describe the theoretical framework, including the spin models for the relevant degrees of freedom, and the framework to calculate PL. We discuss both a 4-spin-model and a simpler 2-spin-model, proposed in reference 8, and how they are related. In section III we present our simulations for the PL of neutral quantum dots. We consider both band-to-band transitions, such that the final state is the neutral acceptor A^0 , and the band-to-acceptor transition, such that the final state is h^+A^- , i.e. a QD hole interacting with the spin $S = 5/2$ of the ionized Mn acceptor. We find that an antiferromagnetic QD hole-Mn coupling can still yield an effective ferromagnetic coupling between the QD hole and the Mn-acceptor complex (consisting on the Mn ion and the acceptor hole), as observed by Kudelski *et al.*⁸. In section IV we present our results for negatively charged quantum dots. In this case, since there are two electrons and two holes, there are 2 recombination pathways and 4 possible sets of PL spectra are possible. In section V we summarize the main results.

II. THEORETICAL FRAMEWORK

A. Photoluminescence and eigenstates

Our goal is to extract information of the quantum state of the single Mn spin in the quantum dot from optical spectroscopy data. We adopt a phenomenological approach where only the spin degrees of freedom of the Mn, quantum dot (QD) carriers and acceptor hole are considered. The various spin couplings are chosen to respect the symmetries of the problem and are fitted to experimental data when available. The relevant electronic states of the quantum dot are described in terms of few-spin quantum states which depend on the different spin exchange interactions.

In the calculation of the PL, it is convenient to distinguish between the ground state and the exciton state manifolds¹³. Both the number of states and the effective spin Hamiltonian of these manifolds depend on the charge of the dot^{7,11} and on the charge state of the acceptor complex. For instance, the relevant degrees of freedom of the ground state manifold (GSM) of a neutral QD are the spins of the Mn spin and the acceptor hole. The exciton state manifold (XSM) enlarges the GSM with the addition of the QD electron and the QD hole. By definition, the GSM is defined by the eigenstates of the Hamiltonian of the dot before the photoexciton is injected:

$$\mathcal{H}_G|\Psi_G\rangle = E_G|\Psi_G\rangle \quad (1)$$

In the case of Mn in a neutral InAs QD, G runs over the 24 possible states that can be formed with a spin $S = 5/2$ of the Mn and a pseudospin $3/2$ of the acceptor. Notice that E_G takes different values (ground state

spin splittings) due to either exchange coupling between the Mn and the acceptor hole or, in the case of compensated impurities or II-VI semiconductors, coupling to an external field. The XSM is formed by the eigenstates of the exciton Hamiltonian, which can be written as the sum of \mathcal{H}_G and the new terms involving all the couplings of the photocarriers with the degrees of freedom before excitation:

$$\mathcal{H}_X|\Psi_X\rangle = E_X|\Psi_X\rangle \quad (2)$$

Both E_X and E_G and their wavefunctions are obtained from diagonalization of the model Hamiltonians described below in detail.

The PL spectrum for a given polarization state λ is related to these states¹³:

$$I_\lambda(\omega) = \sum_{X,G} n_X |\langle \Psi_G | \mathcal{P}_\lambda | \Psi_X \rangle|^2 \delta[\hbar\omega - (E_X - E_G)] \quad (3)$$

Here n_X is the probability that a given XSM state is occupied and $\langle \Psi_G | \mathcal{P}_\lambda | \Psi_X \rangle$ are the the matrix elements, of the interband electric dipole operator¹³ that promotes an electron from the valence states to the conduction states and viceversa. This operator obeys the standard optical selection rules associated to the photon with polarization λ and does not affect the Mn spin state. Explicit expressions of this operator are provided once we discuss the nature of \mathcal{H}_G and \mathcal{H}_X and their eigenvectors.

In a non-magnetic dot, the PL spectrum has a single line at zero magnetic field. A distinctive feature of magnetically doped dots is the appearance of several lines at zero magnetic field^{6,7,8}. According to equation (3) the appearance of several lines in the PL spectra can occur both due to splittings in the GSM and in the XSM. The intensity of the lines depends on two factors, the quantum mechanical matrix elements and the statistical occupation of the emitting state, n_X . This quantity depends on the complicated non-equilibrium kinetics of the photoinjected carriers. Instead of solving a non-equilibrium master equation¹¹, we assume that the emitting states are in a thermal equilibrium with an effective temperature which can be larger than the temperature of the lattice. This phenomenological approach is supported by experimental results in the case of single Mn in a CdTe QD⁶.

B. 4-spin-model

1. Ground State Manifold

Mn has two s electrons which participate in the sp -bonding, whereas In has three. Therefore, substitutional Mn in InAs behaves like an acceptor. EPR¹⁶ and photoemission¹⁷ experiments indicate that Mn retains the five d electrons when doping concentrations are small. Hence, Mn keeps an oxidation state of +2 resulting in an effective charge of -1 , that repels the electrons

nearby. The Mn impurity remains charge neutral, at the scale of a few unit cells, by binding a hole. The binding energy of the hole is of 110 meV in Ga(Mn)As^{18,19} and 28 meV in In(Mn)As^{5,20}. The acceptor hole state has a radius of approximately 1 nm and has been probed by STM experiments both in GaAs² and InAs⁵. In bulk the acceptor hole has a fourfold degeneracy inherited from the top of the valence band, which is lifted by quantum confinement and/or strain. Because of the strong spin-orbit interaction, it is convenient to treat the acceptor hole as a spin $j = 3/2$ object, exchange coupled to the Mn spin $M = 5/2$.

The operators acting upon this object are the four by four $J = 3/2$ angular momentum matrices, \vec{j} . In the spherical approximation²¹ the Mn-acceptor hole spin coupling reads²²:

$$\mathcal{H}_{M,j} = \epsilon \vec{M} \cdot \vec{j} \quad (4)$$

where $\epsilon = +5$ meV is the antiferromagnetic coupling between the acceptor hole and the Mn, \vec{M} are the $S = 5/2$ spin matrices of the Mn and \vec{j} are the $J = 3/2$ matrices corresponding to the total angular momentum of the valence band states. The Hamiltonian equation (4) is readily diagonalized in the basis of the total spin $F = M + J$, the spin of the Mn plus acceptor hole complex. F can take integer values between 1 and 4. The eigenvalues are $E(F) = \frac{\epsilon}{2}F(F+1) + E_0$. Since the coupling is antiferromagnetic, the ground state has $F = 1$, separated from the $F = 2$ states by a relatively large energy barrier of 2ϵ . Hence, as long as the Mn-acceptor hole complex is not distorted by perturbations that couple different F manifolds and temperature is low enough, it is a good approximation to think of it as being a composite object with total spin $F = 1$. Since they play an important role, we explicitly write down the 3 wave functions of the $F = 1$ manifold:

$$\begin{aligned} |1, +1\rangle &= \frac{1}{\sqrt{2}} \left| \frac{5}{2}, \frac{-3}{2} \right\rangle - \frac{\sqrt{30}}{10} \left| \frac{3}{2}, \frac{-1}{2} \right\rangle + \\ &\quad + \frac{\sqrt{15}}{10} \left| \frac{1}{2}, \frac{1}{2} \right\rangle - \frac{\sqrt{5}}{10} \left| \frac{-1}{2}, \frac{3}{2} \right\rangle \\ |1, 0\rangle &= \frac{1}{\sqrt{5}} \left| \frac{3}{2}, \frac{-3}{2} \right\rangle - \frac{\sqrt{30}}{10} \left| \frac{1}{2}, \frac{-1}{2} \right\rangle + \\ &\quad + \frac{\sqrt{30}}{10} \left| \frac{-1}{2}, \frac{-1}{2} \right\rangle - \frac{1}{\sqrt{5}} \left| \frac{-3}{2}, \frac{3}{2} \right\rangle \\ |1, -1\rangle &= \frac{-1}{\sqrt{2}} \left| \frac{-5}{2}, \frac{3}{2} \right\rangle + \frac{\sqrt{30}}{10} \left| \frac{-3}{2}, \frac{1}{2} \right\rangle - \\ &\quad - \frac{\sqrt{15}}{10} \left| \frac{-1}{2}, \frac{-1}{2} \right\rangle + \frac{\sqrt{5}}{10} \left| \frac{1}{2}, \frac{-3}{2} \right\rangle \end{aligned} \quad (5)$$

where we use the notation

$$|F = 1, F_z = \pm 1, 0\rangle = \sum_{M_z, j_z} C_{M_z, j_z}(F, F_z) |M_z, j_z\rangle$$

We see that because of the very strong exchange interaction between the acceptor hole and the Mn spins, their

spins are strongly correlated and they are not good quantum numbers separately.

Following Govorov²³, we assume that the QD is larger than the bulk acceptor state. Thus, the QD perturbs weakly the acceptor state. In this approximation we can distinguish between quantum confined or QD states and acceptor states. The former are extended all over the dot the latter are tightly bound to the Mn impurity and their energy lies in the gap (see figure 1). The opposite scenario, in which the QD size is comparable or smaller than the acceptor state, has been considered by Climente et al.²⁴, would yield different results incompatible with the experiments of Kudelski *et al.*⁸, as discussed below.

The cubic symmetry of the ideal crystal and the presence of quantum confinement and strain result in additional terms in the Hamiltonian, that need to be summed to equation (4). Both quantum dot confinement and strain can result in a splitting of the light and heavy hole bands, that can be modelled a $-Dj_z^2$ term. This term would be present in thin film layers with strain and still preserves rotational invariance in the xy plane. The presence of the quantum dot potential will break this in plane symmetry. To lowest order²⁵ this can be modelled by an additional term in the Hamiltonian, $E(j_x^2 - j_y^2)$. Notice that we assume that these perturbations act on the acceptor state only and not on the Mn d electrons. This is justified since the hole is spread over tens of unit cells, whereas the Mn d states are confined within an unit cell. Hence, we take the following model for the ground state Hamiltonian:

$$\mathcal{H}_G = \epsilon \vec{M} \cdot \vec{j} - Dj_z^2 + E(j_x^2 - j_y^2) \quad (6)$$

As we discuss below we have $\epsilon \gg D \gg E$. Within the $F = 1$ lowest energy manifold the D term splits the triplet into a $F_z = \pm 1$ doublet and a $F_z = 0$ singlet. The E term hybridizes the $F_z = \pm 1$ states, resulting in a small hybridization splitting.

We obtain the the eigenstates of \mathcal{H}_G by expressing them as linear combinations of $|M_z, j_z\rangle = |M_z\rangle \otimes |j_z\rangle$:

$$|\Psi_G\rangle = \sum_{M_z, j_z} \mathcal{C}_{M_z, j_z}^G |M_z, j_z\rangle = \sum_{F, F_z} \mathcal{D}_{F, F_z}^G |F, F_z\rangle \quad (7)$$

and diagonalizing numerically the Hamiltonian matrix. The use of the $|F, F_z\rangle$ basis might be better for interpretation of the results.

Finally, in some instances we need to consider the ionized acceptor complex, h^+A^- . This is the case if we consider the band-to-acceptor transition in neutral dots or if we consider a charged quantum dot. The spin of the Mn inside the A^- state is $M = 5/2$ and should have properties similar to those of Mn in CdTe⁶.

2. Exciton state manifold

We now consider states with an electron and a hole in the QD lowest energy levels in the conduction and

valence band respectively (see figure 1). In contrast to the case of neutral Mn in II-VI semiconductor, the exciton states involves 4 spins instead of three: the Mn ($M = 5/2$), the QD conduction electron $\sigma_c = \pm 1/2$, the QD hole $\sigma_h = \pm 3/2$ and the acceptor hole $J = 3/2$. Since we ignore LH-HH mixing for the QD valence states, the QD holes are heavy hole, with well defined $J_z = \pm 3/2$ (or \uparrow, \downarrow). As a result, the spin couplings of the QD to the other spins (Mn, acceptor hole and QD electron) are Ising like. Including the small LH-HH mixing present in the QD hole state results in a small spin-flip terms in the exchange Hamiltonian of the QD hole¹¹. We label the hole spin states as the time reversed states of the valence electronic Bloch states with quantum number σ_v ²⁶, $\sigma_h = -\sigma_v$. With this notation, the spin of a given state that features one quasiparticle in the valence band, either one electron or one hole, is the same as the spin of the quasiparticle. With this notation, the exciton spin X satisfies the rule $X = \sigma_h + \sigma_c$ and takes values ± 1 states for optically active excitons and ± 2 for optically dark excitons^{26,27}.

Since we have 4 spin degrees of freedom we need to consider the 6 two spin couplings between them:

$$\mathcal{H}_X = \mathcal{H}_G + \mathcal{H}_{c,h} + \mathcal{H}_{h,M} + \mathcal{H}_{h,j} + \mathcal{H}_{c,M} + \mathcal{H}_{c,j} + \mathcal{H}_Z \quad (8)$$

One of them, the $\vec{M} \cdot \vec{j}$ term, is present both in the GSM and XSM. The symmetry and the coupling strength characterize a given spin-spin interaction. In spin rotational invariant systems two spins \vec{s}_1 and \vec{s}_2 interact via Heisenberg coupling, $\vec{s}_1 \cdot \vec{s}_2$. When the interplay of spin-orbit coupling and lack of spherical symmetry break spin rotational symmetry, spins are coupled with different strengths along different directions. An extreme case are flat self-assembled quantum dots, for which the lowest energy hole states are purely heavy holes such that in-plane couplings are strictly forbidden¹³, resulting in Ising couplings. In the opposite limit, the conduction band states and the Mn d states have no orbital momentum which greatly reduces the size of spin-orbit interactions, resulting in Heisenberg couplings between each other. An intermediate situation would be that of holes in spherical nanocrystals, where, in spite of strong spin orbit interactions, Mn-hole exchange is still described with a Heisenberg coupling²⁸. Following previous work in CdTe^{11,13}, we take the QD hole-Mn and the QD electron-Mn coupling as antiferromagnetic Ising and ferromagnetic Heisenberg respectively.

The second term in equation (8) is the longitudinal QD electron-hole exchange that splits the bright ± 1 and dark ± 2 excitons in two doublets:

$$H_{eh} = +J_{eh}\sigma_c\sigma_h \quad (9)$$

Since the dark doublet, for which $\sigma_c\sigma_h > 0$ is lower in energy we have $J_{eh} < 0$. For simplicity, we neglect transverse electron-hole exchange.

In the case of A^0 we also need to include the coupling of the QD electron and QD hole spins both to the Mn spin

and to the acceptor hole. We assume the same symmetry for the two couplings:

$$\mathcal{H}_{hM} + \mathcal{H}_{hj} = J_{hM}\sigma_h M_z + J_{hj}\sigma_h j_z \quad (10)$$

Notice that the sign of the hole-hole coupling is not clear a priori. The QD conduction electron couplings are:

$$\mathcal{H}_{cM} + \mathcal{H}_{cj} = -J_{cM}\vec{\sigma}_c \cdot \vec{M} - J_{cj}\vec{\sigma}_c \cdot \vec{j} \quad (11)$$

Finally, we include the Zeeman coupling of the various spins to an external magnetic field. For simplicity, we ignore the orbital coupling to the magnetic field. In the neutral dot there are 2 spins in the GSM and 4 spins in the XSM that are coupled to the magnetic field. Thus, we need 4 g -matrices. In this paper we only consider magnetic fields along the growth axis. The couplings read:

$$\mathcal{H}_Z = \mu_B B_z (g_c\sigma_c + g_h\sigma_h + g_M M_z + g_j j_z) \quad (12)$$

where $\mu_B = \frac{\hbar e}{2m} = +0.0579$ meV/T.

The exciton states in the 4-spin-model are obtained by numerical diagonalization of the Hamiltonian. We express them as linear combinations of the product basis $|M_z, j_z, \sigma_c, \sigma_h\rangle$:

$$|\Psi_X\rangle = \sum_{M_z, j_z, \sigma_c, \sigma_h} \mathcal{C}_{M_z, j_z, \sigma_c, \sigma_h}^X |M_z, j_z, \sigma_c, \sigma_h\rangle \quad (13)$$

The 4-spin-model has 96 eigenstates, as many as the product of the $(2S+1) \times (2J+1) \times 4$, where $2S+1=6$ is the multiplicity of the Mn spin, $2J+1=4$ is the multiplicity of the acceptor hole spin, and 4 is the number possible of quantum dot exciton states.

The eigenvalues and eigenvectors of \mathcal{H}_X depend on the strength of the spin couplings. These depend both on the material and the sample. For instance, exchange coupling between the QD carriers to the Mn spin is given by the product of the material exchange integrals¹⁴, α and β , and the probability amplitude of the QD envelope functions for either electrons or holes^{13,15}, which is clearly a sample dependent property. For the same reason, the hole-Mn coupling is much stronger for the acceptor state than for the QD state. Here we choose the numerical values of the exchange coupling constants to account for the experimental data. Sample to sample variations will result in different PL spectra.

Importantly, as long as the Mn-acceptor hole is the dominant coupling, there are 12 lowest energy exciton states, well separated from the rest. These 12 states correspond to the possible combinations of the 4 exciton states and the 3 $F=1$ states. Although these states are predominantly $F=1$, they are somewhat mixed with higher F states. It must be noted that, assuming a thermal occupation with an effective temperature, the PL is predominantly given by transitions from the $F=1$ manifold.

C. 2-spin-model

The 4-spin-model has as much as 6 exchange constants which might not be possible to extract from comparison with PL experiments. The situation can be significantly simplified trading off some accuracy. In the GSM, we can remove the $F > 1$ states as long as they are not thermally occupied ($k_B T < 2\epsilon$) and not mixed dynamically through the terms that break rotational symmetry, i.e. as long as both D and E are also much smaller than 2ϵ . If these conditions are met, we can use a single spin model for the ground state⁸. The 3 by 3 Hamiltonian in the $F = 1$ subspace reads:

$$\mathcal{H}_G = -\mathcal{D}F_z^2 + \mathcal{E}(F_x^2 - F_y^2) + g_F \mu_B F_z B_z \quad (14)$$

A Hamiltonian similar to this has been used to model Mn in GaAs quantum wells²⁹. The coupling constants of the 2-spin-model are obtained from those of the 4-spin-model by representing equations (6) and (12) in the basis set of the $F = 1$ states from equation (5). We obtain

$$\begin{aligned} \mathcal{D} &= \frac{3}{10}D \\ \mathcal{E} &= \frac{3}{10}E \\ g_F &= \frac{7}{4}g_M - \frac{3}{4}g_j \end{aligned} \quad (15)$$

The \mathcal{D} term splits the $F = 1$ triplet into a singlet $|1, 0\rangle$ and a doublet, $|1, \pm 1\rangle$. The \mathcal{E} term mixes the two states in the ± 1 doublet resulting in a bonding and anti-bonding states along the Y and X axis respectively.

Along the same lines, the XSM Hamiltonian can be approximated by a simpler 2-spin-model one, if we treat the optically active exciton as a quantum Ising degree of freedom, $X_z = \pm 1$, coupled to the spin $F = 1$ formed by the Mn spin and the acceptor hole. In that case, the XSM Hamiltonian reads:

$$\mathcal{H}_X = \mathcal{H}_G + \mathcal{J}F_z X_z + g_X \mu_B X_z B_z \quad (16)$$

The strength of the effective exciton Mn complex coupling is related to the bare coupling constants of the 4-spin-model through:

$$\begin{aligned} \mathcal{J} &= \frac{21}{8}J_{hM} - \frac{9}{8}J_{hj} \\ g_X &= \frac{3}{2}g_h - \frac{1}{2}g_c \end{aligned} \quad (17)$$

In obtaining equation (17) we set the electron-Mn complex interaction to zero. It is worth noting that the sign of g_F , the effective g -factor of the effective composite spin F , as well as the sign of \mathcal{J} , the effective exciton-Mn complex coupling, could be different from those of the constituent particles. In particular, even if both the QD hole-acceptor hole J_{hj} and the QD hole-Mn couplings J_{hM} are antiferromagnetic, we could have a negative (ferromagnetic) effective coupling if $J_{hj} > \frac{7}{3}J_{hM}$. This sign

reversal occurs because the very strong Mn-acceptor hole interaction distorts their wave functions and perturbs their couplings to a third spin.

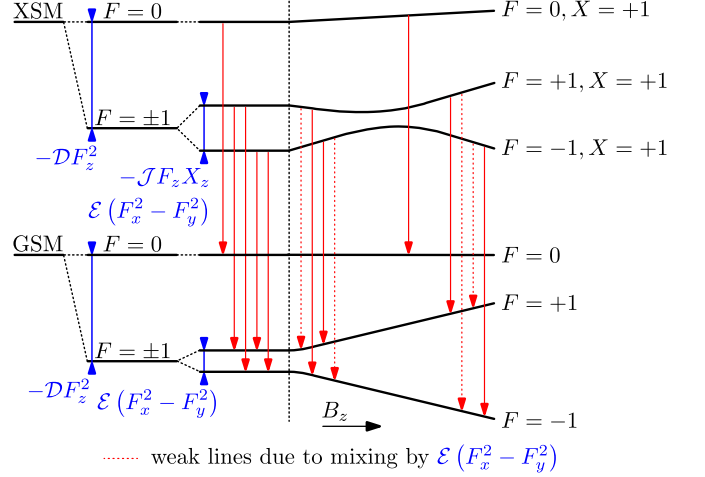


FIG. 2: Energy level diagram for the neutral exciton band-to-band transitions. Both the ground state and exciton state ($X = +1$) energy lines are shown, as well as their evolution as a function of the magnetic field. (Color online)

The advantage of the 2-spin-model is that it can be solved analytically. The details are provided in the appendix. Importantly, the $F_z = 0$ state is decoupled from the $F_z = \pm 1$ pair, both in the GSM and the XSM. The energy level diagram is shown in the figure (2). The GSM features a weakly split doublet. The energy separation with the higher energy $F_z = 0$ singlet is \mathcal{D} . The doublet, denoted x and y , is a linear combination of the $F_z = \pm 1$ states. The small splitting within the doublet is approximately equal to \mathcal{E} . The Zeeman term affects the $F_z = \pm 1$ states.

Since in the 2-spin-model the $F_z = 0$ state is decoupled from the $F_z = \pm 1$ states, it is convenient to think of the doublet $|F = 1, F_z = \pm 1\rangle$ as a isospin 1/2 space. Both the exchange coupling and the applied field (in the Faraday geometry) act as effective magnetic fields along the isospin z axis, whereas the \mathcal{E} term acts an effective magnetic field in the isospin xy plane. In the 2-spin-model the bright exciton does not shift the $F_z = 0$ state. Thus, the exciton exchange and the magnetic field mix the x and y wave functions of the $F_z = \pm 1$ doublet. The mixing opens two new optical transitions, marked in the diagram of figure (2).

D. Optical selection rules

We now discuss the selection rules associated to the dipole \mathcal{P}_λ operators that we need to use in equation (3). They promote an electron from the valence band to the conduction band and viceversa. In a Mn doped III-V QD there are two relevant valence band levels so that exciton recombination can occur through two channels,

as shown in figure 1: band-to-band and band-to-acceptor. These transitions have different energies and, since the wavefunctions of these holes are not the same, different optical selection rules.

Emission of a σ^+ (σ^-) photon in the direction normal to the QD layer takes away (adds) one unit of angular momentum L_z from the system. In the band-to-band transitions we shall ignore LH-HH mixing of the quantum dot hole state. Therefore, emission of a σ^+ (σ^-) implies the removal of the +1 (-1) exciton. Hence, in the band-to-band channel, the transition operators are defined from its action upon XSM states as a projector:

$$\begin{aligned}\mathcal{P}_-|\Psi_X\rangle &= \sum_{M_z, j_z} \mathcal{C}_{M_z, j_z, \uparrow, \Psi}^X |M, j_z\rangle \\ \mathcal{P}_+|\Psi_X\rangle &= \sum_{M_z, j_z} \mathcal{C}_{M_z, j_z, \downarrow, \uparrow}^X |M_z, j_z\rangle\end{aligned}\quad (18)$$

We omit the prefactor proportional to the single particle dipole matrix element, which is a convolution of the atomic and the envelope wave functions. Ignoring LH-HH mixing in the band-to-band transition implies that, in our model, linear polarization can only occur through quantum coherence between the +1 and -1 exciton.

In the band-to-acceptor transition the dipole operator moves an electron from the QD conduction level to the acceptor level, for which we can not ignore LH-HH mixing. Hence the gain (loss) of one unit of angular momentum upon σ^+ (σ^-) photon emission can occur also through the light hole channel. Thus, in a band-to-acceptor transition the spin of the annihilated conduction band electron σ_c and the acceptor hole j_z are given to the σ^\pm photon:

$$\sigma_c + j_z = \pm 1 \quad (19)$$

The band-to-acceptor transition operator \mathcal{P}_\pm is fully described by its action upon a given state $|\Psi_X\rangle$ of the XSM. The resulting GSM state read, for σ^+ emission:

$$\begin{aligned}\mathcal{P}_+|\Psi_X\rangle &= \sum_{M_z, \sigma_h} \mathcal{C}_{M_z, +3/2, \downarrow, \sigma_h}^X |M_z\rangle \otimes |\sigma_h\rangle + \\ &+ \frac{1}{\sqrt{3}} \mathcal{C}_{M_z, +1/2, \uparrow, \sigma_h}^X |M_z\rangle \otimes |\sigma_h\rangle\end{aligned}\quad (20)$$

and for σ^- emission:

$$\begin{aligned}\mathcal{P}_-|\Psi_X\rangle &= \sum_{M_z, \sigma_h} \mathcal{C}_{M_z, -3/2, \uparrow, \sigma_h}^X |M_z\rangle \otimes |\sigma_h\rangle + \\ &+ \frac{1}{\sqrt{3}} \mathcal{C}_{M_z, -1/2, \downarrow, \sigma_h}^X |M_z\rangle \otimes |\sigma_h\rangle\end{aligned}\quad (21)$$

Notice that these operators leave the quantum dot hole unchanged and connect states in which the Mn spin is strongly coupled to the acceptor hole to states where the acceptor hole is compensated and the Mn spin is only coupled to the QD hole. Notice that, both in band-to-band and band-to-acceptor transitions, the dipole operators do not act on the Mn d electrons. Therefore, the

spin of the Mn is conserved during the photon emission processes. This is in contrast to intra-shell transitions relevant when the bandgap is larger than the intra-atomic transitions³⁰.

III. NEUTRAL EXCITON SPECTROSCOPY

We now present our calculations for the PL spectra for neutral InAs quantum dots doped with one Mn. We consider both band-to-band $X^0 A^0 \rightarrow A^0$ and band-to-acceptor $X^0 A^0 \rightarrow h^+ A^-$ transitions. The symmetry of the state left behind after photon emission is very different in these two cases. In reference 8 the band-to-band transition $X^0 A^0 \rightarrow A^0$ has been experimentally observed and described with a model very similar to the one presented in the previous section. We first revisit this case which permits to obtain numerical values for the parameters in the Hamiltonian. This makes it possible to address the band-to-acceptor transition for which there is no experimental data and no available prediction of how the PL spectra should look like.

A. Band-to-band transitions: 4-spin-model

In the band-to-band transition the system is left in one of the GSM states discussed in the previous section where the Mn-acceptor hole complex behaves like a $F = 1$ spin. In band-to-band transitions the spin A^0 complex is probed by the quantum dot exciton. This is the scenario considered by Kudelski *et al.*⁸. Here we compute the PL spectrum by numerical diagonalization of the GSM and the XSM within the 4-spin-model and then combining equations (3) and the polarization operator equation (18). We use the numerical values of the coupling constants in the 4-spin-model as to fit the experimental PL spectrum of reference 8. The experimental zero field PL features 5 lines: a central low intensity one in between a high and a low energy doublet. Both the $B_z = 0$ zero field PL and the PL as a function of energy and applied field in the Faraday geometry are shown in figure 3. Our calculations, shown in figure (3), reproduce the zero field PL⁸ with 5 peaks at zero magnetic field, as well as the main features of the PL as a function of magnetic field. Notice that in the horizontal axis we plot with respect to E_0 the transition energy of the bare quantum dot exciton, excluding its coupling to the Mn.

The origin of the 5 peaks at zero field can be understood by inspection of the energy diagram shown in figure (2) (see also reference 8), in which we only show states within the $F = 1$ manifold. The basic idea is that the quantum dot exciton is probing the F_z component of a spin $F = 1$ object. If F_z was a good quantum number, 3 lines should be expected: the middle peak, corresponding to $F_z = 0$, and a high and low energy peaks, corresponding to the spin splitting of the $F_z = \pm 1$ states Ising coupled to the exciton spin. However, the

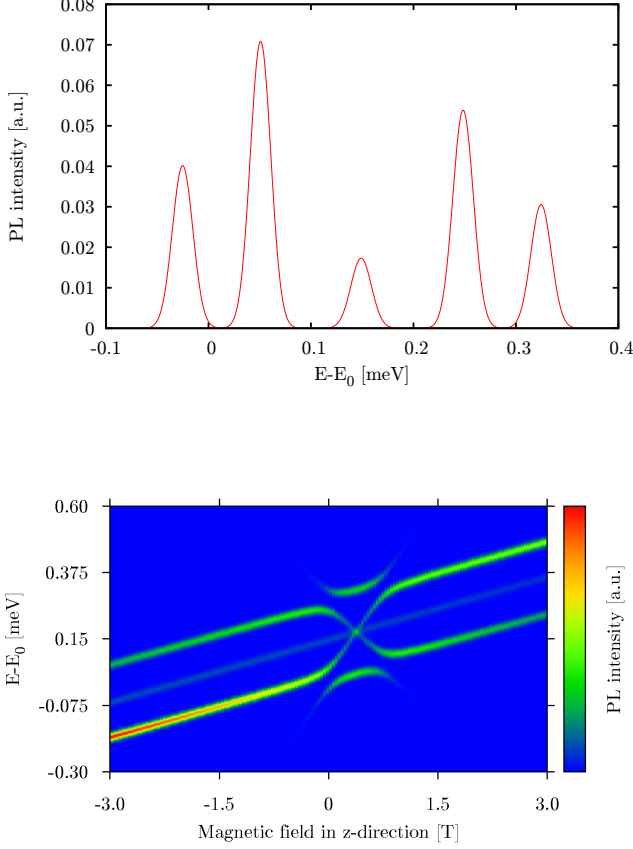


FIG. 3: Neutral exciton band-to-band transition calculated with the 4-spin-model. Upper panel: $B_z = 0$ σ^+ -PL. Lower panel: color plot of σ^+ -PL intensity as function of energy (vertical axis) and applied magnetic field (horizontal axis). (Color online)

in-plane anisotropy results in the mixing states within the $F_z = \pm 1$ doublet into x and y states with slightly different energies. As a result, there are direct (xx, yy) transitions as well as crossed transitions (xy, yx). The fact that the height of the xx and xy transitions are similar denotes that the exchange interaction is comparable to the in-plane anisotropy term E . The energy difference between these satellite ($F_z = \pm 1$) transitions and the $F_z = 0$ central peak arises from the exchange coupling to the exciton.

The origin of the reduced intensity of the $F_z = 0$ central peak is not in the quantum mechanical matrix elements, but in the smaller statistical occupation probability, given that the $F_z = 0$ state has a higher energy than the $F_z = \pm 1$ doublet. Interestingly, since there are no transitions mixing $F_z = \pm 1$ to $F_z = 0$, D can not be inferred directly from PL line splittings. In contrast, the value of D strongly affects the intensity of the central peak. We estimate $D \simeq 4$ meV.

These results are different from single Mn doped CdTe quantum dots, for which the PL has 6 peaks at zero field.

There the QD exciton is probing the M_z component of a spin 5/2 object without in-plane magnetic anisotropies. Here the 5 peaks show the interaction of a QD exciton with a spin $F = 1$ object with in-plane magnetic anisotropy.

Additional information is obtained from the evolution of the PL spectra as a function of an applied magnetic field along the growth axis z . In the experiment⁸ the 5 lines seen at zero field evolve, changing both in intensity and energy, in an intricate manner. In figure the lower panel of (3) we show a contour plot of the PL intensity as a function of energy (vertical axis) and magnetic field (horizontal axis) for σ^+ transitions, obtained within the 4-spin model. The fact that the calculation is in fairly good agreement with the experiment, and provides a strong back up for the theory.

B. Band-to-band transitions: 2-spin-model

We now discuss the physical interpretation of the evolution of the PL spectra as a function of the applied magnetic field using the 2-spin-model proposed by Kudelsy *et al.*⁸. The 2-spin-model affords analytical expressions for the PL spectrum at finite magnetic field in the Faraday configuration. The derivation is shown in the appendix. We address the merger of 3 lines at a particular value of the applied field, B^* , the non-monotonic evolution of the highest and lowest energy lines at small field and the quenching of their intensity at large fields. Within this model a given circular polarization of the photon fixes the QD exciton spin. There are 3 exciton states and 3 ground states. The $F_z = 0$ state, both for the XSM and the GSM, is decoupled from the other states and gives rise to the central line. The Zeeman shift of this line is that of the QD exciton, $g_X \mu_B B_z$. Thus, we can fit the experimental data⁸ and infer from here the g -factor of the QD exciton $g_X = 1.2$ not far from values reported before³¹.

The other four lines come from transitions within the $F_z = \pm 1$ doublets. The energy levels of the ground state $F_z = \pm 1$ doublet are given by $-\mathcal{D} \pm h_G$ where

$$h_G = \sqrt{\mathcal{E}^2 + (g_F \mu_B B_z)^2} \quad (22)$$

The energy levels of the $F_z = \pm 1$ doublet in the XSM with exciton spin $X_z = \pm 1$ are given by $E_0 - \mathcal{D} + g_X \mu_B X_z B_z \pm h_X$ where E_0 is the exciton energy transition without spin and Zeeman terms and

$$h_X = \sqrt{\mathcal{E}^2 + (g_F \mu_B B_z + J X_z)^2} \quad (23)$$

Both in the GSM and XSM the two states in the doublet are linear combination of both $F_z = +1$ and $F_z = -1$. The mixing between the $F_z = \pm 1$ states is governed by the competition between the in-plane anisotropy \mathcal{E} , and the longitudinal interactions of the F_z spin with the applied field and, in the exciton manifold, the exchange

coupling to the exciton. This competition can be described by two angles, $\cot \theta_G = \frac{g_F \mu_B B_z}{\mathcal{E}}$ and $\cot \theta_X = \frac{g_F \mu_B B_z + \mathcal{J} X_z}{\mathcal{E}}$. Due to the different mixing in the GSM and XSM, 4 transitions are allowed. We label them with ba , where $a = \pm$ and $b = \pm$ label the low (-) and high (+) energy state of the ground and exciton state in the $F_z = \pm 1$ manifold. From equation (A13) we have the transition energies

$$E^{b \rightarrow a} = E_0 + g_X \mu_B X_z B_z + b h_X - a h_G \quad (24)$$

At $B_z = 0$ we have $h_X = \sqrt{\mathcal{E}^2 + (\mathcal{J} X_z)^2}$ and $h_G = \mathcal{E}$, so that $h_X - h_G > 0$. Thus, from the $B_z = 0$ point we immediately can label the 4 non-monotonic lines from low to high energy, at zero field, as $-+$ (1), $--$ (2), $++$ (3) and $+-$ (4). We also denote with (0) the central line with $F_z = 0$. The splitting between the two low (high) energy lines is $2h_G$ and their average energy is $-h_X$ ($+h_X$). At zero field $h_G = \mathcal{E}$, thus \mathcal{E} is half the splitting within both the low and the high energy doublets. We thus infer $\mathcal{E} = 0.035$ meV. The splitting between the high energy doublet and the low energy doublet is, at zero field, $2h_X = \sqrt{\mathcal{J}^2 + \mathcal{E}^2}$. From here we infer $|\mathcal{J}| = 0.14$ meV.

Equation (24) permits to extract the field B^* at which lines (2), (3) and (0) cross. The crossing arises from the compensation between the Zeeman splitting of the F spin and its exchange coupling to the exciton. The condition is $h_X = h_G$ is satisfied for

$$2g_F \mu_B B^* = -\mathcal{J} X_z \quad (25)$$

Since B^* is positive for $X_z = +1$ we immediately see that \mathcal{J} must be negative: the F_z spin is ferromagnetically coupled to the QD exciton. As discussed earlier, the negative sign can be obtained even if in the 4-spin-model the QD hole-Mn coupling is antiferromagnetic. Thus, the negative sign comes from the strong correlation between the Mn spin and the acceptor hole spin, such that the sign of F_z and M_z are anticorrelated in the $F = 1$ manifold. In the simulations with the 4-spin model we have used positive values for the QD hole-Mn coupling, obtaining good agreement with the experiment. Since we can infer \mathcal{J} from the $B_z = 0$ data, equation (25) permits to infer g_F from the experimental value of B^* . We obtain $g_F = 3.01$, not far from the $g_F = 2.77$ of Mn-acceptor complex in GaAs.

The intensity of the 4 lines in the $F_z = \pm 1$ manifold are a function of $\alpha \equiv \frac{1}{2}(\theta_G - \theta_X)$ (see equation A13). In particular, the strength of $++$ and $--$ transitions is given by $\cos^2(\alpha)$ whereas the strength of the $+-$ and $-+$ transitions is given by $\sin^2(\alpha)$. In the high field limit, when $g_F \mu_B B_z \gg |\mathcal{J} X_z|$, we have $\theta_X = \theta_G$ and α goes to zero. In figure (4) we plot the σ^+ PL spectra. The size and color of the circles is proportional to the quantum yield equation (A13). The quantum yield of the $F_z = 0$ transition is constant. The slope of this line, coming from the Zeeman splitting of the QD exciton, is also present in the other four lines.

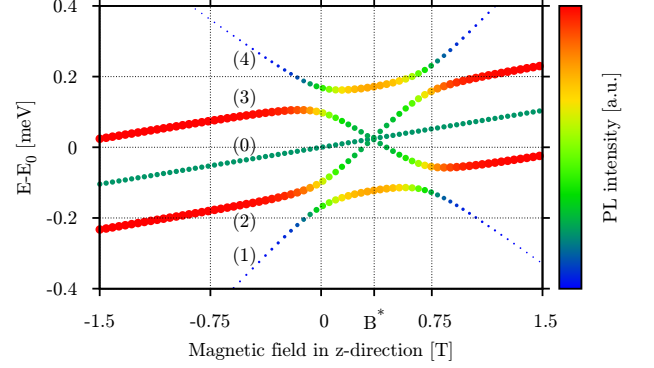


FIG. 4: σ^+ -PL intensity of the neutral exciton band-to-band transition, as a function of the magnetic field, calculated with the 2-spin-model (eq. A12). Thermal effects are not included. The size and color of the symbols of the numbered lines is proportional to the quantum yield. The intensity of the central line is constant. (Color online)

Lines (1) and (4) come from transitions that mix $+$ and $-$ states with different symmetry. Their energy with respect to line (0) is given by $\pm(h_X + h_G)$. Since $\mathcal{J} < 0$, h_X has a minimum at $B_z = B^*$ whereas h_G , whose contribution is smaller, has a minimum at $B_z = 0$. The intensity of these lines quenches as the magnetic field increases so much that $g_F \mu_B B_z \gg \mathcal{E}$ and the F_z is restored as a good quantum number. In contrast, lines (2) and (3) come from $++$ and $--$ transitions. At large fields the quantum yield is increased since the mixing between $F_z = +1$ and -1 is quenched. The energy of (2) and (3) with respect to (0) is given by $\pm(h_X - h_G)$. Thus, when the Zeeman splitting is much larger than the exchange coupling, i.e. for $B_z \gg 2B^*$, we have $h_X \simeq h_G$ and the slope of lines (2) and (3) is the same as (0).

The model captures the main experimental features of the PL spectrum⁸, namely: *i*) 5 peaks distributed as a high and low energy doublets with a small intensity central peak; *ii*) as a magnetic field is applied along the growth direction, the central line does not change intensity and has a linear shift, whereas the doublets have non-monotonic shifts and do change intensity, two of them fade away; *iii*) at a given value of B^* 3 lines, coming from the low and high doublets and the central line, cross.

The results of the 2-spin-model (figure 4) and 4-spin-model (figure 3) have no apparent differences (besides the lack of thermal occupation in the 2-spin-model). This validates the approximations made to go from the 4-spin-model to the 2-spin-model.

The model portrays the neutral Mn acceptor complex in InAs as a spin $F = 1$ nanomagnet with two almost degenerate ground states, $F_z = \pm 1$, a rather large single ion magnetic anisotropy of \mathcal{D} , and a small in-plane anisotropy \mathcal{E} . The quantum dot exciton is Ising coupled to F_z and permits a direct measurement of \mathcal{E} and \mathcal{J} ,

and indirect measurement of \mathcal{D} . Finally, we have verified that the model proposed by Climente *et al.*²⁴ could *not* account for the experimental PL reported by Kudelski *et al.*. In a nutshell, this model is very close to the one proposed by one of us to account for the PL of Mn doped charged CdTe quantum dots⁷. In the model of Climente *et al.*, the ground state manifold has 6 doublets coming from the Ising coupling of the hole and the Mn spin. The injection of an additional electron-hole pair will result in two holes with opposite spin occupying the same orbital, uncoupled from the Mn, which would interact only with the electron, presumably via a Heisenberg coupling. Thus, the exciton manifold of such a model would have two spectral lines. The resulting spectrum would have 11 lines with a characteristic V shape⁷. If the Mn-electron coupling is turned off, the model yields 6 equally strong lines.

C. Band-to-acceptor transition

We now consider band-to-acceptor transitions, $X^0 A^0 \rightarrow h^+ A^-$ such that, after photon emission there is a hole left in the QD levels and the Mn is liberated from the acceptor hole. This kind of transition has been observed in Mn doped GaAs bulk³² and quantum wells³³ but not yet in Mn doped quantum dots. Three obvious differences with the band-to-band transitions can be mentioned beforehand. Firstly, the PL spectrum associated to the acceptor transition should be red-shifted with respect to the band-to-band transition, by the sum of the acceptor binding energy and the quantum dot confinement energy. In GaMnAs quantum wells the reported shift is approximately 107 meV³³. Secondly, we expect a smaller intrinsic efficiency of the band-to-acceptor process compared to the band-to-band case, due to the smaller electron-hole overlap in the case of the former. Thirdly, the final state, $A^- h^+$ is an excited state since the QD hole could be promoted to the acceptor state, reducing the energy of the system. The spin of the $A^- h^+$ state is the product of the Mn spin $S = 5/2$ and the QD hole spin.

A diagram of the energy levels of this transition is shown in figure (5). The states of the XSM are the same as in the band-to-band transition, except for the fact that now both the $X = \pm 1$ and the $X = \pm 2$ transitions are allowed, since the optical selection rule must be enforced with the acceptor hole and not with the QD hole. Quantum dot electron-hole exchange splits the “dark” and “bright” lines. Thus, in the lowest energy $F = 1$ manifold there are 6 energy lines in the XSM corresponding to 3 projections of F_z and the two excitons.

The GSM features now an ionized Mn acceptor interacting with a quantum dot hole instead of with an acceptor hole. Both the strength and the symmetry of this coupling are different: the QD hole-Mn coupling is much weaker than acceptor hole-Mn coupling and, due to the lack of spherical symmetry of the QD hole state, is pre-

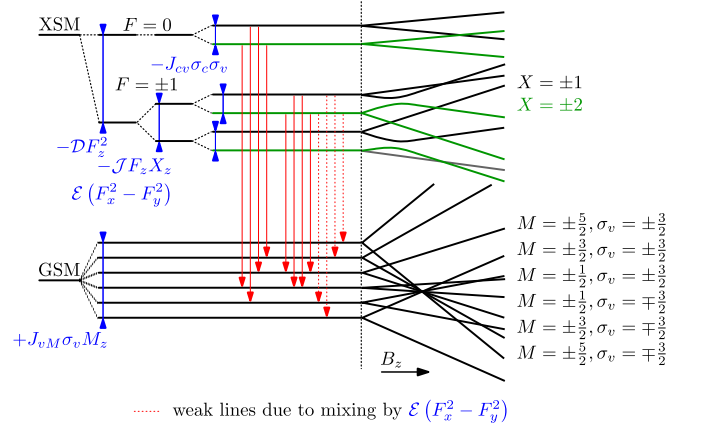


FIG. 5: Energy level diagram for the neutral exciton band-to-acceptor transitions. Both the ground state and exciton state energy lines are shown, as well as their evolution as a function of the magnetic field. (Color online)

dominantly Ising^{6,13}. Hence, the GSM is given by the Ising coupling of the ionized Mn, with spin $S = 5/2$ and the QD hole, with total angular momentum $\sigma_h = \pm 3/2$. The spectrum of this system, relevant for single Mn in CdTe QD^{11,13}, is formed by six doublets. We can label the GSM states with the projections of the Mn spin and the QD hole spin along the growth axis, $|M_z, \sigma_h\rangle$. Their eigenvalues are:

$$E_{M_z, \sigma_h} = +J_{hM}^G M_z \sigma_h. \quad (26)$$

where J_{hM}^G is the exchange coupling between the QD hole and the ionized Mn spin.

There could be as many as 36 PL spectral lines joining the 6 energy levels of the XSM and the 6 energy levels in the GSM. The highest energy PL would correspond to the highest energy exciton state (within the $F = 1$ manifold), with quantum numbers $F_z = 0$, $X = \pm 1$ and the lowest energy ground state, with quantum numbers $M_z = +5/2, \sigma_h = -3/2$ or $M_z = -5/2, \sigma_h = +3/2$. Interestingly, the $M_z = \pm 5/2$ state has zero overlap with the $F_z = 0$, so that this particular transition is forbidden (see figure 5). Going up in the M_z ladder, the first excited states in the GSM are $M_z = +3/2, \sigma_h = -1/2$ and $M_z = -3/2, \sigma_h = +1/2$.

The results of the simulation within the 4-spin-model are shown in figure (6). Using values from the band to band transition we take $D = 4.7$ meV, $E = 0.31$ meV, $\epsilon = 5$ meV, $J_{hM} = -0.0405$ meV, $J_{eh} = -0.2$ meV. We assume that the QD hole-acceptor hole coupling is zero, but we take a ferromagnetic coupling between the Mn and the QD hole to reproduce the effective ferromagnetic coupling between the exciton and the Mn acceptor complex. In the ground state we take a QD hole-Mn coupling larger than that of the XSM to account for the larger electrostatic attraction of the ionized Mn acceptor, $J_{hM}^G = 0.15$ meV. The PL features a group of higher intensity lines at low energy and a group of weaker lines 2 meV

above. As we discuss below, the splitting between the low and the high energy groups turns out to be given by $\mathcal{D} = 3D/10$. Thus, band-to-acceptor transitions would permit a direct spectroscopic measurement of D . The V shape of the intensity pattern in the low energy group is somewhat related to the PL spectra of charged Mn-doped CdTe quantum dots⁷. In both cases the optical matrix elements feature overlap between states with well defined Mn spin and states where the Mn spin is Heisenberg exchanged coupled to another carrier (the extra electron in Mn doped CdTe and the acceptor hole in the case considered here).

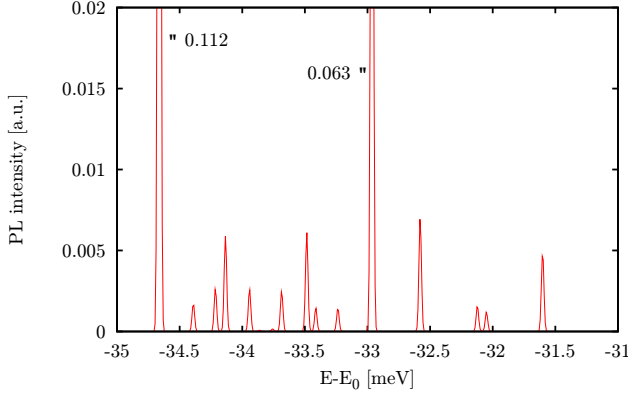


FIG. 6: $B_z = 0$ σ^+ -PL for neutral exciton band-to-acceptor transition, as calculated with the 4-spin-model. (Color online)

D. Band-to-acceptor transition: 2-spin-model

The results of figure (6) can be rationalized with the 2-spin-model, like in the band-to-band transition. We describe exciton states as the product of the QD electron-hole pair spin, which can be ± 2 or ± 1 times the acceptor complex spin $F_z = \pm 1, 0$. We ignore, for a moment, the in-plane anisotropy term \mathcal{E} that mixes $F_z = \pm 1$. Thus F_z , σ_c and σ_h are good quantum numbers in the XSM and M_z and σ_h are good quantum numbers in the GSM. Of course, the spin of the QD hole, σ_h , and the Mn spin, M , are conserved during the transition.

The quantum matrix elements of these transitions are given by the matrix elements of the dipole operator (eq. 20 and 21) between emitting states, X and ground states with quantum numbers M_z, σ_h :

$$|\langle M_z, \sigma_h | \mathcal{P}_+ | \Psi_X \rangle|^2 = |\mathcal{C}_{M_z, +3/2, \downarrow, \sigma_h}^X + \frac{1}{\sqrt{3}} \mathcal{C}_{M_z, +1/2, \uparrow, \sigma_h}^X|^2$$

$$|\langle M_z, \sigma_h | \mathcal{P}_- | \Psi_X \rangle|^2 = |\mathcal{C}_{M_z, -3/2, \uparrow, \sigma_h}^X + \frac{1}{\sqrt{3}} \mathcal{C}_{M_z, -1/2, \downarrow, \sigma_h}^X|^2$$

for the σ^+ and σ^- transitions respectively. Ignoring the in-plane mixing term \mathcal{E} , for a given QD exciton (σ_c, σ_h),

the coefficients $\mathcal{C}_{M_z, j_h, \sigma_c, \sigma_h}^X$ are given by equation (5). Thus, as long as F_z is a good quantum number, the spin of the acceptor hole and the Mn satisfies the rule

$$M_z = F_z - j_z \quad (27)$$

Thus, for a given state in the XSM, with quantum numbers $|F = 1, F_z, \sigma_c, \sigma_h\rangle$, and a given polarization of the photon, ± 1 , we immediately get the permitted values of the annihilated acceptor hole spin $j_z = \pm 1 - \sigma_c$ (eq. 19) and the allowed values of the Mn spin after photon emission (eq. 27).

Using equations (5), (19), (27) one can make a table where the inputs are the QD electron spin σ_c , the acceptor complex spin F_z , the circular polarization of the photon σ^\pm , and the outputs are the annihilated acceptor hole spin j_z , the Mn spin M_z after photon recombination and the quantum yield of the transition, $\mathcal{I} \equiv I(F_z, \sigma_c, \sigma^\pm, M_z)$. For σ^+ polarization we obtain:

F_z	σ_c	j_z	M_z	$\mathcal{I}(\sigma^+)$
+1	\uparrow	+1/2	+1/2	5/100
0	\uparrow	+1/2	-1/2	10/100
-1	\uparrow	+1/2	-3/2	10/100
+1	\downarrow	+3/2	-1/2	5/100
0	\downarrow	+3/2	-3/2	20/100
-1	\downarrow	+3/2	-5/2	50/100

The table for σ^- is obtained by application of the time reversal operator, which changes F_z, σ_c, j_z, M_z , to $-F_z, -\sigma_c, -j_z, -M_z$, and give the same intensity. In order to get the PL spectrum we need the transition energies $E_X - E_G$. Neglecting the \mathcal{E} term that mixes $F_z = \pm 1$, the XSM energies are approximated by

$$E_X(F_z, \sigma_c, \sigma_h) = E_0 - \mathcal{D}F_z^2 + \mathcal{J}X_zF_z + J_{eh}\sigma_c\sigma_h \quad (29)$$

and the energy of the ground states by equation (26). Thus, the transition energies $\omega = E_X - E_G$ are given by:

$$\omega = E_0 - \mathcal{D}F_z^2 + \mathcal{J}(\sigma_c + \sigma_h)F_z + \sigma_h(J_{eh}\sigma_c - J_{hM}^G M_z) \quad (30)$$

In figure (7) we plot the intensity of the lines, without thermal depletion of the higher energy $F_z = 0$ states. The numerical values of the constants are those of the 4-spin-model simulation, properly renormalized to the 2-spin-model. Thus we take $\mathcal{D} = 3D/10 = 1.41$ meV, $\mathcal{J} = \frac{21J_{hM}}{8} = -0.12$ meV. The numerical values of the QD electron-hole exchange and the QD hole-Mn coupling in the ground state are the same in the 2-spin and 4-spin models, $J_{eh} = -0.2$ meV and $J_{hM}^G = +0.15$ meV. We take $J_{hM}^G > \mathcal{J}$ because the quantum dot hole is electrostatically attracted towards the Mn when this is ionized. The PL of figure (7) features 12 peaks, corresponding to the 6 allowed transitions of equation (28) times the two possible spin orientations of the QD hole. The high energy group corresponds to the transitions coming from the $F_z = 0$ states. Most of the splitting between the high and the low energy group is given by \mathcal{D} , with some contribution coming from the exciton Mn-complex exchange.

The lower energy group of 8 peaks correspond to transitions in the $F_z = \pm 1$ manifold. The high intensity peaks correspond to transitions where the Mn spin is left in a $\pm 5/2$ state. For σ^+ transitions, shown in the figure, the peaks correspond to final states with $M_z = -5/2$ and the quantum dot hole with spin $+1/2$ (low energy peak) and $-1/2$ (high energy peak). The splitting between those two is $\frac{5J_{eM}}{2} + \frac{J_{eh}}{2} - \mathcal{J}$. Interestingly, this simple model captures the main features of the PL, as calculated with the 4-spin-model. The latter has more lines because of the \mathcal{E} terms, that mix $F_z = 1$ to the $F_z = -1$ terms.

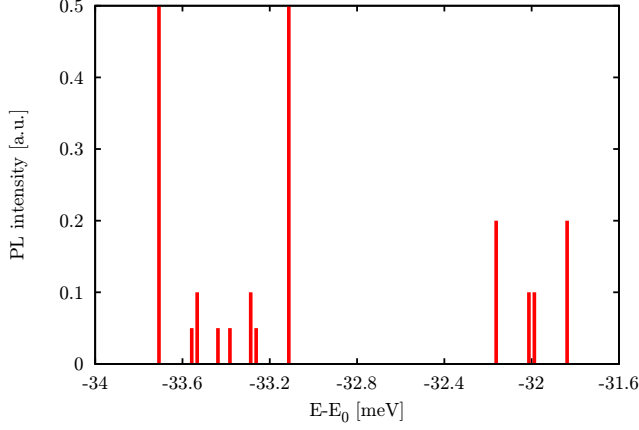


FIG. 7: $B_z = 0$ σ^+ -PL for neutral exciton band-to-acceptor transition, calculated with the 2-spin-model with $\mathcal{E} = 0$ (see text). (Color online)

It is worth noting that the band-to-acceptor transitions permit to relate the degree of spontaneous circular polarization to a possible imbalance in the F_z population^{33,34,35}. For instance, the transitions that have as initial state $F_z = -1$, averaged over all the possible QD spin orientation and final state have a degree of circular polarization of more than 70 percent:

$$\frac{\sum_{M_z, \sigma_c} (I(-1, \sigma_c, M_z, +) - I(-1, \sigma_c, M_z, -))}{\sum_{M_z, \sigma_c} (I(-1, \sigma_c, M_z, +) + I(-1, \sigma_c, M_z, -))} = \frac{5}{7} \quad (31)$$

Thus the degree of Mn spin polarization can be probed by measuring the degree of circular polarization of the PL.

Hence, whereas band-to-band transitions probe the Mn-acceptor complex, which behaves as a spin $F = 1$ object, the band-to-acceptor transitions connect initial states for which the Mn spin is correlated to the acceptor hole to final states where the Mn spin is Ising coupled to the QD hole, but with M_z as a good quantum number. In band-to-acceptor transitions the photon energy and polarization carry information about M_z .

IV. CHARGED EXCITON SPECTROSCOPY

We now consider the PL spectra of negatively charged InAs dots. From the theory side there is a lot of interest on the effect of number of carriers on the magnetic properties of a dot doped with Mn atoms^{9,11,15,24,36,37,38}. A priori, the ground state of a negatively charged InAs dot doped with a single Mn should be the ionized A^- acceptor, with spin properties identical to those of Mn in neutral CdTe¹³. Band-to-band transitions should yield zero field PL spectra with 6 peaks. Band-to-acceptor transitions for the negatively charged dot, $e^- A^0 \rightarrow A^-$, have been studied by A. Govorov in reference 23. He obtained a PL spectrum with 3 peaks in at zero magnetic field.

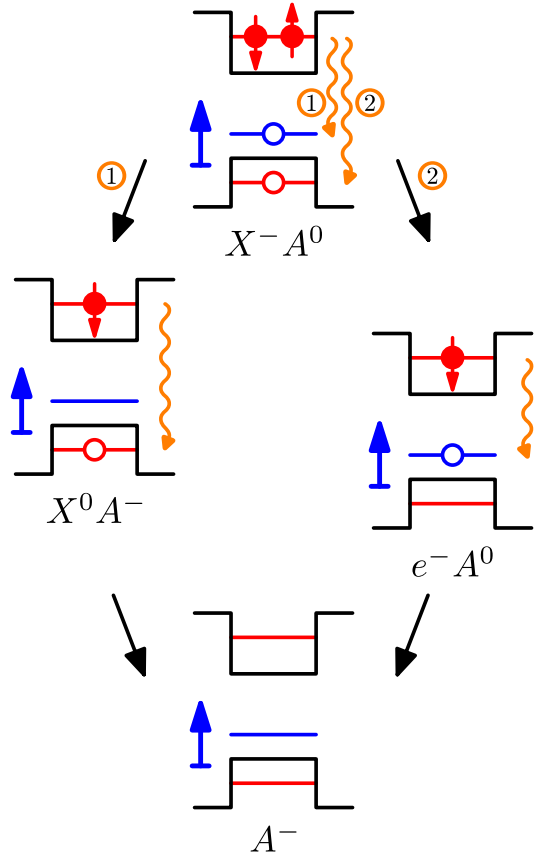


FIG. 8: Possible electronic configurations for two photon decay of the negatively charged InAs QD with one Mn. The uppermost diagram shows the configuration with two QD electrons, one QD hole and the neutral Mn-acceptor hole complex. By a band-to-acceptor transition (pathway 1), one arrives at one of the intermediate configurations, with an ionized Mn and a QD exciton. A further band-to-band transition, creates the lowest energy configuration: an ionized Mn. Another recombination possibility is via pathway 2: a band-to-band transition yields the intermediate configuration with the neutral Mn-acceptor complex and one QD electron. A further band-to-acceptor transition then yields the same end configuration as the one achieved via pathway 1. (Color online)

Contrary to these expectations, the experimental results on negatively charged single Mn doped InAs QD⁸ show very similar neutral and charged exciton band-to-band spectra, with 5 peaks in the zero field PL. The reported transitions correspond to an emitting state with a neutral Mn acceptor plus a quantum dot trion (X^-A^0). Thus, there are two electrons in the conduction level, and two holes, the acceptor hole and the QD hole (see figure 8). The final state, after the emission of two photons, is the ionized Mn, with spin $S = 5/2$. The fact that the reported neutral and negatively charged transitions are very similar indicates that QD electrons are very weakly coupled to the Mn-acceptor hole complex. This is different from CdTe dots doped with one Mn, where the addition of a single electron changes the spin properties of the Mn^{7,11,15}. In InAs, the Mn is strongly coupled to the acceptor hole and is less sensitive to the number of conduction band carriers.

Yet the presence of additional QD electrons can result in new PL spectra when we consider band-to-acceptor transitions, unreported so far in single Mn-doped InAs quantum dots. Since the negatively charged trion X^-A^0 features 2 electrons and 2 holes in different states, the decay towards the ground state A^- can occur via two recombination pathways, as shown in figure 8. One of the pathways (denoted as 1 in the figure) consist in a band-to-acceptor transition $X^-A^0 \rightarrow X^0A^-$ followed by a $X^0A^- \rightarrow A^-$, i.e., a band-to-band transition that annihilates a QD exciton coupled to a ionized Mn acceptor. The PL of the first step in pathway 1 is related to the band-to-acceptor transition of the neutral dot discussed in the previous section. The PL of the second step in pathway 1 should be very similar to that of single Mn doped CdTe QD. As long as the Ising part of the coupling between the QD hole and the Mn spin is dominant, as in CdTe, the PL of the energy and polarization of the photon yield direct information of the Mn spin after the exciton recombination¹³.

Pathway 2 in the figure starts with a band-to-band transition $X^-A^0 \rightarrow e^-A^0$ followed by a band-to-acceptor transition $e^-A^0 \rightarrow A^-$. The first step has been observed experimentally and, since the electron-Mn exchange is very weak, yields a PL very similar to the neutral case considered above. The second step is identical to the transition considered by Govorov²³.

In the upper panel of figure (9) we show the zero field PL for the band-to-acceptor transition for negatively charged InAs QD doped with 1 Mn. The emitting state is X^-A^0 and the final state is X^0A^- , a quantum dot exciton coupled to an ionized Mn acceptor. The corresponding energy level diagram is very similar to that of the neutral band-to acceptor transition shown in figure (5). Ignoring states with $F > 1$, there are 6 exciton states, corresponding to 3 F_z values and 2 QD hole spin states. There are 24 ground states, corresponding to the 6 Mn spin orientations and the 4 spin states of the quantum dot exciton. This is in contrast with the $X^0A^0 \rightarrow h^+A^-$ transition, for which both the GSM and the XSM have 12

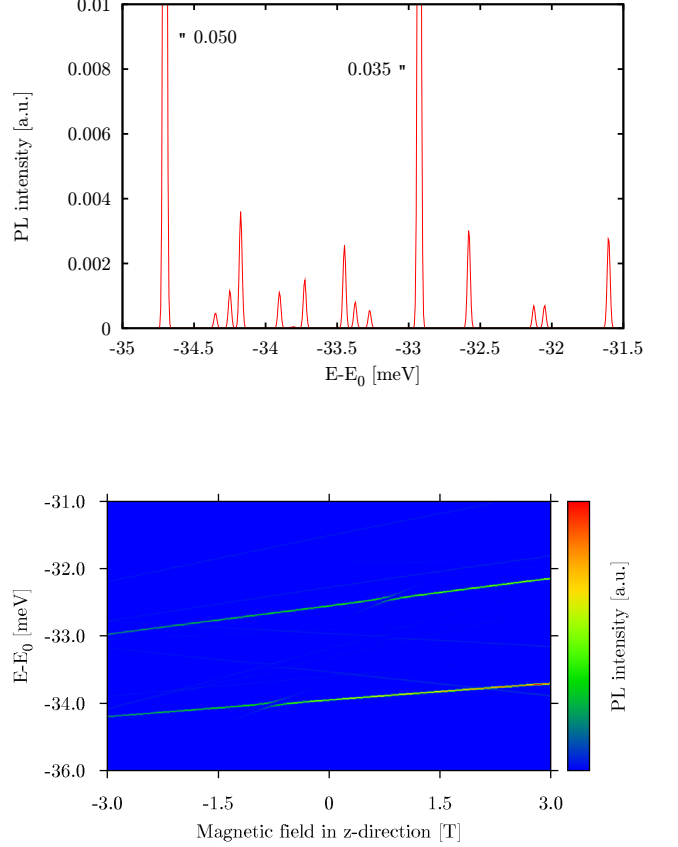


FIG. 9: Upper panel: $B_z = 0$ σ^+ -PL for a negatively charged exciton band-to-acceptor transition ($X^-A^0 \rightarrow X^0A^-$), as calculated with the 4-spin-model. Lower panel: Intensity plot for the σ^+ -PL for the negatively charged exciton band-to-acceptor transition ($X^-A^0 \rightarrow X^0A^-$), as a function of energy (vertical axis) and applied magnetic field (horizontal axis). (Color online)

states. Other differences with that transition is the lack of QD electron-hole exchange in the emitting state, and the presence of that coupling in the ground state. Thus, electron-hole exchange is present both in the neutral and in the charged case, either in the XSM or in the GSM. It would be possible to do an analytical model for the charged case along the lines of the previous section for which the optical matrix elements would be still given by equation (28). Not surprisingly, the PL $X^-A^0 \rightarrow X^0A^-$ of figure (9), calculated with the 4-spin-model, is quite similar to that of the $X^0A^0 \rightarrow h^+A^-$.

In the lower panel of figure (9) we plot the σ^+ PL as a function of the magnetic field in the Faraday configuration. The two low energy brighter peaks correspond to transitions where the Mn spin is, in the final state $M_z = -5/2$. They are splitted due to the different spin orientations of the QD exciton to which they are coupled. This results also in different slopes as the magnetic field is ramped. The evolution of the energy levels in the ground

state results in a compensation of the zero field exchange splittings by the finite field Zeeman splittings. At a particular value of the magnetic field, several lines become degenerate. In the absence of spin-flip terms, they do not anti-cross. This particular energy arrangement has been reported in CdTe doped with Mn⁶. The anti-crossings observed at $B_z \simeq 1\text{T}$ are related to those taking place at the XSM and discussed above in the context of neutral band-to-band transitions.

V. DISCUSSION AND CONCLUSIONS

We have addressed the problem of single exciton spectroscopy of a single-Mn InAs doped quantum dot. The main goal is to link a few-spin Hamiltonian with the PL spectra featuring spin-split peaks at zero magnetic field. We have focused on the fact that, for single Mn-doped InAs QD this is a 4 body problem, with the QD electron, QD hole, acceptor hole and Mn spin. In order to account for the experimental observations⁸ it is important to assume that a bulk-like acceptor states survives inside the gap, weakly affected by the quantum dot. The strongest exchange interaction is that of the Mn and the acceptor hole. In most instances this permits to interpret the results as if the quantum dot exciton interacts with a spin $F = 1$ object, obtained from the antiferromagnetic coupling of the Mn spin $S = 5/2$ and the acceptor hole $j = 3/2$. We use both a 4-spin-model, in which the identity of the spin of all the carriers is included in the calculation, and a 2-spin-model, that ignores the composite nature of the exciton and the Mn-acceptor complex. The models are diagonalized numerically and the PL spectra are obtained, taking full account of the optical and spin selection rules.

The 2-spin-model portrays the Mn acceptor complex in InAs as a spin $F = 1$ nanomagnet with two almost degenerate ground states, $F_z = \pm 1$, a rather large single ion magnetic anisotropy of \mathcal{D} , and a small in-plane anisotropy \mathcal{E} . The notion that single Mn atoms in quantum dots can behave like artificial single molecule magnets has been discussed before^{11,39}. Interestingly, the zero field exciton spectroscopy gives a direct measurement of $\mathcal{E} \simeq 0.035\text{ meV}$, but only an indirect measurement of $D \simeq 4\text{ meV}$, through the height of the central peak. The evolution of the PL spectra as a magnetic field is applied permits an indirect measurement of other energy scales in the problem. In the band-to-band transitions, measured by Kudelski et al.⁸, there is particular value of the field B^* at which three lines in the spectra merge. B^* is the field at which the Zeeman splitting and exchange coupling to the exciton have the same intensity and opposite sign (eq. 25). Since the zero field measurement provides \mathcal{J} , the value of g_F in InAs can be inferred from B^* . We estimate $g_F = 3.01$.

The nature of Mn spin $S = 5/2$ can be unveiled in two manners: upon electron doping the system and in band-to-acceptor recombination of the charge neutral dot. The

latter results in the ionization of the Mn complex so that, in the final state, the Mn spin is $S = 5/2$ and is presumably Ising coupled to the QD hole. The band-to-band and band-to-acceptor transitions are very different. In the former the Mn spin is slaved by the acceptor hole both in the XSM and GSM states. Thus, photon emission does not change the symmetry of the Mn spin Hamiltonian. In the band-to-acceptor transition the Mn is liberated from the acceptor hole in the final state, so that photon emission involves a change of the effective Mn spin Hamiltonian. In this sense, the band-to-acceptor transition resembles the negatively charged trion transition in Mn doped CdTe⁷. Band-to-acceptor transitions would provide a direct spectroscopic measurement of \mathcal{D} .

Notice that, within the 2-spin-model we take an effective ferromagnetic coupling between the exciton and the Mn. The 2-spin-model does not say whether this coupling is QD hole-Mn acceptor complex, QD hole-acceptor hole, QD electron-Mn or QD electron-acceptor hole. If we assume that the dominant coupling is between the Mn spin and the QD hole, we could conclude that the coupling is ferromagnetic, at odds with the usual antiferromagnetic coupling of holes and Mn in III-V materials. Interestingly, we have seen how the bare sign of the QD hole-Mn coupling is reversed when going from the 4-spin-model to the 2-spin-model (see equation 17). The strong Mn-acceptor hole complex results in the renormalization of the spin interactions of these two spins with applied field and the exciton spins. This can even result in sign inversion of the exchange interaction. Thus, we have shown that a ferromagnetic coupling between the 2 spins of the simpler model can arise even if the underlying spin couplings of the QD hole to the Mn spin are antiferromagnetic. In this way, we reconcile the standard view about this system, in which the holes are coupled antiferromagnetically to the Mn spin, with the observations⁸.

A single Mn in a quantum dot provides an ideal system to address and control the spin of a single object in a solid state environment. The PL spectra provide valuable information of the effective spin Hamiltonians, for different states of the dot. A Mn atom in a InAs QD behaves like a 3 level system. It might be possible to use the encode a single qubit in the almost degenerate $F_z = \pm 1$ doublet. The presence of higher energy $F_z = 0$ state, acting as a barrier, might block spin relaxation between the ground states. In analogy with the case of electron doped and hole doped quantum dots, it should be possible to manipulate the spin of a single or a few Mn spins in a quantum dot by application of laser pulses.

We acknowledge fruitful discussions with A. Govorov. This work has been financially supported by MEC-Spain (Grants FIS200402356 and the Ramon y Cajal Program) and by Consolider CSD2007-0010 and, in part, by FEDER funds.

APPENDIX A: ANALYTICAL SOLUTION OF THE 2-SPIN-MODEL

Here we provide an analytical solution of the ground state and exciton state manifolds within the 2-spin-model. The GSM has 3 states, but the Hamiltonian can be block diagonalized since the $F_z = 0$ state is decoupled from the $F_z = \pm 1$ doublet. The XSM state has 12 states, corresponding to the 4 spin orientations of the exciton and the 3 states of F_z in the $F = 1$ manifold. Since we consider Ising interaction between the exciton and the F spin, the Hamiltonian of the XSM is also block diagonalized. Importantly, both the GSM and the XSM are each characterized by a single angle, θ_G and θ_X , that characterize the ratio between the in-plane mixing of the $F_z = \pm 1$ components and their splitting, induced both by exchange interaction with the exciton and by Zeeman coupling. As we show here, the lineshape of the PL spectrum depends on $\frac{1}{2}(\theta_X - \theta_G)$.

In the basis $|1, +1\rangle, |1, -1\rangle, |1, 0\rangle$ the Hamiltonian of the GSM reads:

$$\mathcal{H}_G = \begin{pmatrix} -\mathcal{D} + g_F \mu_B B_z & \mathcal{E} & 0 \\ \mathcal{E} & -\mathcal{D} - g_F \mu_B B_z & 0 \\ 0 & 0 & 0 \end{pmatrix} \quad (\text{A1})$$

We can write the two by two matrix within the $F_z = \pm 1$ subspace as a linear combination of the unit matrix \mathbf{I} , and the Pauli matrices σ_z and σ_x :

$$\mathcal{H}_{G,\pm 1} = -\mathcal{D}\mathbf{I} + \vec{h}_G (\cos(\theta_G)\sigma_z + \sin(\theta_G)\sigma_x) \quad (\text{A2})$$

with

$$\vec{h}_G = (\mathcal{E}, g_F \mu_B B_z) = h_G (\sin(\theta_G), \cos(\theta_G)) \quad (\text{A3})$$

where $h_G = \sqrt{\mathcal{E}^2 + (g_F \mu_B B_z)^2}$. Thus, we have

$$\cot(\theta_G) = \frac{g_F \mu_B B_z}{\mathcal{E}} \quad (\text{A4})$$

At zero field we have $\theta_G = \pi/2$.

The eigenvalues of the GSM are: $-\mathcal{D} - h_G$, $-\mathcal{D} + h_G$ and 0. The corresponding eigenvectors are the product the quantum dot ground state, denoted by $|0\rangle$, and the spin part, denoted by Ψ_G^-, Ψ_G^+ and Ψ_G^0 respectively. The spin part of the $F_z = \pm 1$ sector reads

$$\begin{pmatrix} \Psi_G^- \\ \Psi_G^+ \end{pmatrix} = \begin{pmatrix} \sin\left(\frac{\theta_G}{2}\right) & -\cos\left(\frac{\theta_G}{2}\right) \\ \cos\left(\frac{\theta_G}{2}\right) & \sin\left(\frac{\theta_G}{2}\right) \end{pmatrix} \begin{pmatrix} |1, +1\rangle \\ |1, -1\rangle \end{pmatrix} \quad (\text{A5})$$

Notice that, in the limit of very strong field, $g_F \mu_B B_z \gg \mathcal{E}$, the mixing between $F_z = +1$ and -1 vanishes.

We now consider the XSM, which is split in 4 sectors with 3 states each and a well defined exciton state $X_z = \pm 1$ and $X_z = \pm 2$. We focus on the optically active excitons, $X_z = \pm 1$. Since X_z commutes with the XSM Hamiltonian, the $X_z = -1$ and $X_z = +1$ sectors decouple and are described by 3 by 3 matrices with the same structure as (A1). The $F_z = 0 \otimes X_z$ states are

decoupled from the $F_z = \pm 1 \otimes X_z$ states. In the basis $|1, +1\rangle \otimes |X_z\rangle$, $|1, -1\rangle \otimes |X_z\rangle$ the XSM Hamiltonian for exciton X_z reads:

$$\mathcal{H}_{X_z=\pm 1} = (E(X_z) - \mathcal{D})\mathbf{I} + \vec{h}_X (\cos(\theta_X)\sigma_z + \sin(\theta_X)\sigma_x) \quad (\text{A6})$$

where $E_X(X_z) = E_0 + g_X \mu_B X_z B_z$ is the energy of the excitonic transition neglecting spin couplings plus the QD exciton Zeeman splitting, and

$$\begin{aligned} \vec{h}_X &= (\mathcal{E}, g_F \mu_B B_z + \mathcal{J}X_z) \\ &= h_X (\sin(\theta_X), \cos(\theta_X)) \end{aligned} \quad (\text{A7})$$

where

$$h_X = \sqrt{\mathcal{E}^2 + (g_F \mu_B B_z + \mathcal{J}X_z)^2} \quad (\text{A8})$$

Now we have

$$\cot(\theta_X) = \frac{g_F \mu_B B_z + \mathcal{J}X_z}{\mathcal{E}} \quad (\text{A9})$$

Notice that the angle θ_X depends both on the magnetic field B_z and on the exciton spin projection, $X_z = \pm 1$. At zero field the angles corresponding to $X_z = +1$ and $X_z = -1$ differ by π , so that $\cot(\theta_X) = \pm \frac{\mathcal{J}}{\mathcal{E}}$. At finite fields the effect of exchange and magnetic field on the Mn-acceptor hole complex can either compete or cooperate and the relation between θ_X for $X_z = \pm 1$ is non-trivial.

The eigenvalues are for the XSM are:

$$\begin{aligned} E_0 + g_X \mu_B X_z B_z - \mathcal{D} - h_X \\ E_0 + g_X \mu_B X_z B_z - \mathcal{D} + h_X \\ E_0 + g_X \mu_B X_z B_z \end{aligned} \quad (\text{A10})$$

The corresponding eigenvectors are the product of the quantum dot exciton, denoted by $|X_Z\rangle$ and the spin part, denoted by $\Psi_X^-, \Psi_X^+, \Psi_X^0$ respectively. The spin part of the XSM eigenvectors in the $F_z = \pm 1$ sector are:

$$\begin{pmatrix} \Psi_X^- \\ \Psi_X^+ \end{pmatrix} = \begin{pmatrix} \sin\left(\frac{\theta_X}{2}\right) & -\cos\left(\frac{\theta_X}{2}\right) \\ \cos\left(\frac{\theta_X}{2}\right) & \sin\left(\frac{\theta_X}{2}\right) \end{pmatrix} \begin{pmatrix} |1, +1\rangle \\ |1, -1\rangle \end{pmatrix} \quad (\text{A11})$$

The intensity of the PL lines is given by:

$$I_{\pm}(\omega) = \sum_{a,b} n_b |\langle \Psi_G^a | \Psi_X^b \rangle|^2 \delta(E_X^b - E_G^a + \omega) \quad (\text{A12})$$

where both a and b run over $+1, -1, 0$. Here n_b is the statistical occupation of the exciton states. Both the matrix elements and the allowed transitions depend on the exciton spin $X_z = \pm 1$, which is in turn given by the photon polarization. The intensity table $|\langle \Psi_G^a | \Psi_X^b \rangle|^2$ reads:

Ψ_X	Ψ_G	-	+	0
-	-	$\cos^2\left(\frac{1}{2}(\theta_G - \theta_X)\right)$	$\sin^2\left(\frac{1}{2}(\theta_G - \theta_X)\right)$	0
+	-	$\sin^2\left(\frac{1}{2}(\theta_G - \theta_X)\right)$	$\cos^2\left(\frac{1}{2}(\theta_G - \theta_X)\right)$	0
0	-	0	0	1

This matrix has 5 non-zero elements, corresponding to the 5 permitted transitions for a given circular polarization. The transition energies within the $F_z = \pm 1$ doublets are given by

$$E^{b \rightarrow a} = E_0 + g_X \mu_B X_z B_z + b h_X - a h_G \quad (\text{A13})$$

where both a and b can take values equal to ± 1 .

As expected, the 0 state is decoupled from the others and the optical matrix element is 1. The 4 transitions on

the $F_z = \pm 1$ doublet ($--, -+, +-, ++$) are governed by a single variable $\frac{1}{2}(\theta_G - \theta_X)$. The intensity of the crossed sign transitions goes to zero in the limit of very large fields or exchange coupling. In this situation the mixing induced by in-plane anisotropy term, E , is negligible. Notice that the height of the actual transitions depends both on $|\langle \Psi_G^a | \Psi_X^b \rangle|^2$ and on the statistical occupation. Thus, the observed intensity of the $F_z = 0$ line is smaller, due to a smaller statistical occupation.

-
- ¹ C. F. Hirjibehedin, Chiung-Yuan Lin, Alexander F. Otte, Markus Ternes, Christopher P. Lutz, Barbara A. Jones, Andreas J. Heinrich, *Science* **317**, 1199 (2007)
 - ² A. M. Yakunin, A. Yu. Silov, P. M. Koenraad, J. H. Wolter, W. Van Roy, J. De Boeck, J.-M. Tang, M. E. Flatté, *Phys. Rev. Lett.* **92**, 216806 (2004)
 - ³ D. Kitchen, A. Richardella, J.-M. Tang, M. E. Flatté, A. Yazdani, *Nature* **442**, 436 (2006)
 - ⁴ A. M. Yakunin, A. Yu. Silov, P. M. Koenraad, J.-M. Tang, M. E. Flatté, J.-L. Primus, W. Van Roy, J. De Boeck, A. M. Monakhov, K. S. Romanov, I. E. Panaiotti, N. S. Averkiev, *Nature Materials* **6**, 512 (2007)
 - ⁵ F. Marczinowski, J. Wiebe, J.-M. Tang, M. E. Flatte, F. Meier, M. Morgenstern, R. Wiesendanger, *Phys. Rev. Lett.* **99**, 157202 (2007)
 - ⁶ Y. Léger, L. Besombes, L. Maingault, H. Mariette, *Phys. Rev. Lett.* **93**, 207403 (2004)
 - ⁷ Y. Léger, L. Besombes, J. Fernández-Rossier, L. Maingault, H. Mariette, *Phys. Rev. Lett.* **97**, 107401 (2006)
 - ⁸ A. Kudelski, A. Lemaitre, A. Miard, P. Voisin, T. C. M. Graham, R. J. Warburton, O. Krebs, *Phys. Rev. Lett.* **99**, 247209 (2007)
 - ⁹ A. Efros, E. Rashba, M. Rosen, *Phys. Rev. Lett.* **87**, 206601 (2001)
 - ¹⁰ A. O. Govorov, A. V. Kalameitsev *Phys. Rev. B* **71**, 035338 (2005)
 - ¹¹ J. Fernández-Rossier, R. Aguado, *Phys. Rev. Lett.* **98**, 106805 (2007)
 - ¹² E. C. Steven, L. Zu, M. I. Haftel, A. L. Efros, T. A. Kennedy, D. J. Norris, *Nature* **436**, 91 (2005)
 - ¹³ J. Fernández-Rossier, *Phys. Rev. B* **73**, 045301 (2006)
 - ¹⁴ J. K. Furdyna, *J. Appl. Phys.* **64** R29 (1988)
 - ¹⁵ J. Fernández-Rossier, L. Brey, *Phys. Rev. Lett.* **93** 117201 (2004)
 - ¹⁶ J. Szczytko, A. Twardowski, M. Palczewska, R. Jaboski, J. Furdyna, H. Munekata, *Phys. Rev. B* **63**, 085315 (2001)
 - ¹⁷ J. Okabayashi, T. Mizokawa, D. D. Sarma, A. Fujimori, T. Slupinski, A. Oiwa, H. Munekata, *Phys. Rev. B* **65**, 161203(R) (2002)
 - ¹⁸ M. Ilegems, R. Dingle, L. W. Rupp Jr., *J. of Appl. Phys.* **46**, 3059 (1975)
 - ¹⁹ P. W. Yu, Y. S. Park, *J. of Appl. Phys.* **50**, 1097 (1979)
 - ²⁰ D. G. Andrianov, V. V. Karataev, G. V. Lazareva, Yu B. Muravlev, A. S. Savel'ev, *Sov. Phys. - Semi.* **11**, 738 (1977)
 - ²¹ A. Baldereschi, Nunzio O. Lipari, *Phys. Rev. B* **8**, 2697 (1973)
 - ²² A. K. Bhattacharjee, C. Benoit a la Guillaume, *Solid State Communications* **113**, 17 (2000)
 - ²³ A. O. Govorov, *Phys. Rev. B* **70**, 035321 (2004)
 - ²⁴ J. I. Climente, M. Korkusinski, P. Hawrylak, J. Planelles, *Phys. Rev. B* **71**, 125321 (2005)
 - ²⁵ A. O. Govorov, *Phys. Rev. B* **72**, 075359 (2005)
 - ²⁶ M. Z. Maialle, E. A. de Andrada e Silva, L. J. Sham, *Phys. Rev. B* **47**, 15776 (1993)
 - ²⁷ M. Bayer, G. Ortner, O. Stern, A. Kuther, A. A. Gorbunov, A. Forchel, P. Hawrylak, S. Fafard, K. Hinzer, T. L. Reinecke, S. N. Walck, J. P. Reithmaier, F. Kloppe, F. Schafer, *Phys. Rev. B* **65**, 195315 (2002)
 - ²⁸ A. K. Bhattacharjee, J. Pérez-Conde, *Phys. Rev. B* **68**, 045303 (2003)
 - ²⁹ V. F. Sapega, O. Brandt, M. Ramsteiner, K. H. Ploog, I. E. Panaiotti, N. S. Averkiev, *Phys. Rev. B* **75**, 113310 (2007)
 - ³⁰ N. Que Huong, J. L. Birman, *Phys. Rev. B* **69**, 085321 (2004)
 - ³¹ T. Nakaoka, T. Saito, J. Tatebayashi, and Y. Arakawa, *Phys. Rev. B* **70**, 235337 (2004)
 - ³² Y. Kim, Y. Shon, T. Takamasu, H. Yokoi, *Phys. Rev. B* **71**, 073308 (2005)
 - ³³ R. C. Myers, M. H. Mikkelsen, J. M. Tang, A. C. Gossard, M. E. Flatté, D. D. Awschalom, *Nature Materials* **7**, 203 (2008)
 - ³⁴ N. S. Averkiev, A. A. Gutkin, E. B. Osipov, M. A. Reshchikov, *Sov. Phys. Solid State* **30**, 438 (1988)
 - ³⁵ I. Ya. Karlik, I. A. Merkulov, D. N. Mirlin, L. P. Nikitin, V. I. Perel', V. F. Sapega, *Sov. Phys. Solid State* **24**, 2022 (1982)
 - ³⁶ F. Qu, P. Hawrylak, *Phys. Rev. Lett.* **95**, 217206 (2005)
 - ³⁷ R. M. Abolfath, P. Hawrylak, I. Zutic, *Phys. Rev. Lett.* **98**, 207203 (2007)
 - ³⁸ N. T. Nguyen, F. M. Peeters, *Phys. Rev. B* **76**, 045315 (2007)
 - ³⁹ J. Fernández-Rossier and R. Aguado *Phys. Stat. Sol (c)* **3**, 3734 (2006)